ISSN (Print) 1226-1750
ISSN (Online) 2233-6656
Journal of Magnetics 25(2), 197-204 (2020) https://doi.org/10.4283/JMAG.2020.25.2.197

Effect of Ce and La Substitution on the Microstructure and Magnetic Properties of Hot-deformed Nd-Fe-B Magnets

Ga-Yeong Kim[1,2], Hee-Ryoung Cha[1], Youn-Kyoung Baek[1], Young-Kuk Kim[1], Dong-Hwan Kim[3], Yang-Do Kim[2]*, and Jung-Goo Lee[1]*

[1]Powder & Ceramics Division, Korea Institute of Materials Science, Changwon 51508, Republic of Korea
[2]Department of Materials Science and Engineering, Pusan National University, Busan 46241, Republic of Korea
[3]R&D Center, Star Group, Daegu 42714, Republic of Korea

(Received 12 March 2020, Received in final form 2 June 2020, Accepted 3 June 2020)

Nd in hot-deformed Nd-Fe-B magnets was partially substituted by Ce and La for the purpose of reducing the materials cost and balancing the utilization of rare earth resources. Initial melt-spun ribbons with the nominal compositions of $(Nd_{1-x}M_x)_{13.6}Fe_{bal}B_{5.6}Ga_{0.6}Co_{6.6}$ (x = 0, x = 0.2/M=Ce, x = 0.3/M=Ce, Ce+La, wt.%) were prepared by a single-roller melt-spinning method, and pulverized into powders. The powders were then hot-pressed at 973 K under 100 MPa, and deformed at 973 K until 75 % of height reduction was achieved. The magnetic properties of hot-deformed magnets were decreased with the substitution of Ce for Nd. In addition, simultaneous substitution of Ce and La for Nd resulted in much lower magnetic properties. This tendency was almost the same as initial melt-spun powders. The deterioration on magnetic properties by substation of Ce and La for Nd in hot-deformed Nd-Fe-B magnets could be attributed to not only inferior intrinsic properties of $(Ce/La)_2Fe_{14}B$ to $Nd_2Fe_{14}B$ phase but also the effect of Ce/La substitution on microstructure such as density and grain alignment during hot-deformation. Although the magnetic properties were deteriorated by substitution of Ce and La for Nd in hot-deformed Nd-Fe-B magnets, the cost performance was largely enhanced from 2.32 to 2.62 MGOe×kg/$ by 13 % when increasing the content of Ce substituted for Nd from 0 to 0.3 wt.%.

Keywords : Nd-lean, Nd-Fe-B, hot-deformation, degree of alignment, cost-performance

1. Introduction

Nd-Fe-B magnets are widely used in industrial applications such as the traction motor of hybrid electric vehicles and electric vehicles due to its excellent magnetic properties [1-3]. In general, Nd-Fe-B magnets are composed of ~30 wt.% rare-earth (RE) elements such as Nd, Pr and Dy which are less abundant in the natural rare earth resources. In addition, the rising and unstable cost of these rare earth elements is the most serious problem for Nd-Fe-B magnets to be used in industrial application. On the other hand, Ce and La are the most abundant elements in the natural rare earth resources and their prices are much cheaper than Nd, Pr and Dy. The price of Ce metal is currently about ten times cheaper than Nd metal [4]. Hence, it is a technologically interesting challenge to develop the high performance Nd-lean RE-Fe-B magnets by substitution of Ce and La for Nd, which is also quite important from an industrial viewpoint. Actually, many efforts have been made to investigate the substitution of Ce and La for Nd in sintered Nd-Fe-B magnets [5-7]. However, the magnetic properties of Nd-Fe-B magnets could be drastically deteriorated after replacing Nd with Ce and La due to inferior intrinsic magnetic properties of $Ce_2Fe_{14}B$ ($4\pi M$ = 11.7 kG, H_a = 26 kOe) and $La_2Fe_{14}B$ ($4\pi M$ = 13.8 kG, H_a = 20 kOe) compared to $Nd_2Fe_{14}B$ ($4\pi M$ = 16 kG, H_a = 73 kOe) [8]. Despite of the inferior intrinsic magnetic properties of $Ce_2Fe_{14}B$ and $La_2Fe_{14}B$ to $Nd_2Fe_{14}B$, it is reported that deterioration of magnetic properties due to Ce and La substitution could be largely suppressed by constructing a multi-main-phase (MMP) structure in Nd-lean RE-Fe-B sintered magnets [9]. RE elements are inhomogeneously distributed within 2:14:1 grains during sintering a mixture of Ce, La-free and Ce, La-containing $RE_2Fe_{14}B$ powders. Compared to single-main-phase (SMP) magnets, where Ce and La is

*Co-corresponding author: Tel: +82-55-280-3606
Fax: +82-55-280-3289, e-mail: jglee36@kims.re.kr
e-mail: yangdo@pusan.ac.kr

homogeneously substituted for Nd in the 2:14:1 phase, MMP magnets show much better magnetic performance [10, 11]. On the other hand, there exists secondary phase of $CeFe_2$ with high melting point in Ce-Fe-B magnet. It has been also reported that the $CeFe_2$ phase inevitably forms in the Nd-Ce-Fe-B component with high Ce content [12]. The curie temperature and melting temperature of $CeFe_2$ phase is 235 K and 1198 K, respectively. Therefore, $CeFe_2$ phase is paramagnetic at room temperature and has a poor wettability compared to low melting point RE-rich phase during heat treatment [13-17]. In order to increase the coercivity of Nd-lean RE-Fe-B magnets, it is necessary to carefully control the microstructure such as the grain size and grain boundary [18, 19]. It is reported that grains of a single magnetic domain size (~300 nm), along with grain boundary phase causing sufficient magnetic decoupling among the grains, are the most desirable microstructure to increase coercivity [20]. On the other hand, melt-spinning technique has been employed to obtain ultrafine-grained melt-spun powders, which have high coercivity due to the ultrafine grains but low remanence due to the crystallographically isotropic grains. For the fabrication of anisotropic ultrafine-grained magnets with high maximum energy product, the melt-spun powders should be subjected to the hot-deformation (hot-pressing and subsequent die-upsetting) process. The crystallographic c-axis of grains, which is magnetic easy axis, can be aligned parallel to the pressing direction during the hot-deformation [21]. The grain size of hot-deformed magnets is usually several hundred nanometers, which is one order of magnitude smaller than that of sintered magnets. Hence, hot-deformed magnets have greater potential to achieve higher coercivity compared to sintered magnets.

Although Nd-lean RE-Fe-B magnets have attracted great attention, most of the studies have been concerned with sintered magnets and studies on hot-deformed Nd-lean RE-Fe-B magnet are limited [22, 23]. In this study, therefore, the hot-deformation process was employed to fabricate the anisotropic ultrafine-grained Nd-lean RE-Fe-B magnet using melt-spun powder, and the effect of Ce and La substitution for Nd in RE-FE-B magnet on microstructure and magnetic properties was investigated.

2. Experimental Procedure

Figure 1 shows a schematic diagram of the experimental procedure employed in the present study. Initial ribbons with the nominal compositions of $(Nd_{1-x}M_x)_{13.6}Fe_{bal}B_{5.6}$-$Ga_{0.6}Co_{6.6}$ (x=0, x=0.2/M=Ce, x=0.3/M=Ce and x=0.3/M=Ce+La (ratio = 3:1), wt.%), which named as ND, CE0.2, CE0.3 and CELA0.3, respectively, were prepared by a single-roller melt-spinning method with a wheel speed of 28 m/s in an argon atmosphere, and then pulverized into powder with a particle size of 100 - 300 μm. The composition of ND powder is the same as that of commercial melt-spun powder (MQU-F). The pulverized powders were hot-pressed at 973 K under 100 MPa in a vacuum to prepare cylindrical compacts with 7 mm in diameter and 6 mm in height. The compacts were then subjected to die-upsetting at 973 K with a deformation rate of $\dot{\varepsilon} = 0.1\ s^{-1}$. A deformation degree of $\varepsilon = 1.4$ [$\varepsilon = \ln(h_0/h)$; h_0: starting height of the sample; h: height after deformation] was realized, which corresponds to a 75 % height reduction [24]. The microstructure was investigated using a field emission scanning electron microscopy (FE-SEM). The analysis of phases was carried out by X-ray diffraction (XRD) with CuK_α radiation ($\lambda = 1.5418$ Å). The magnetic properties were measured by vibrating sample magnetometer (VSM) with rectangular parallelepiped specimen [a × b × h (c-axis) = 3 mm × 3 mm × 1 mm] which was prepared from the center of the samples

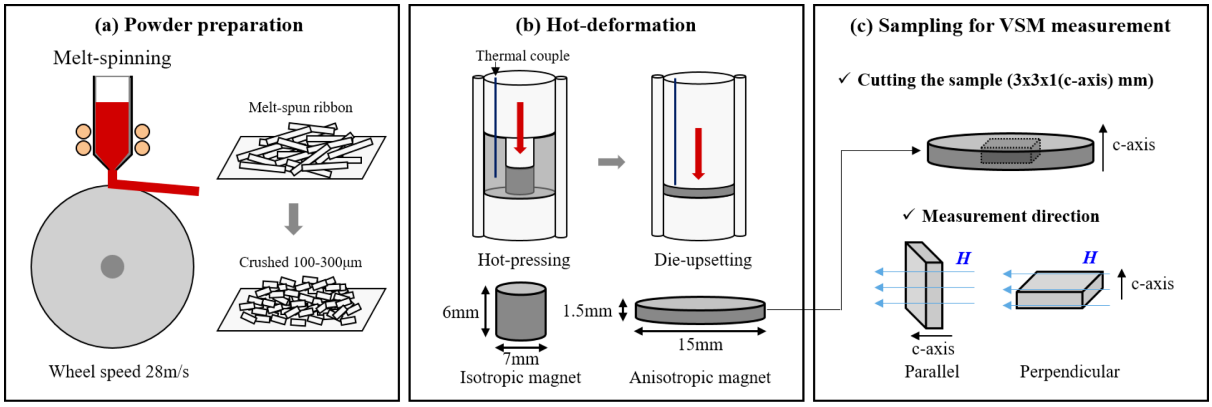

Fig. 1. (Color online) Schematic diagram of (a) powder preparation, (b) hot-deformation and (c) sampling for VSM measurement.

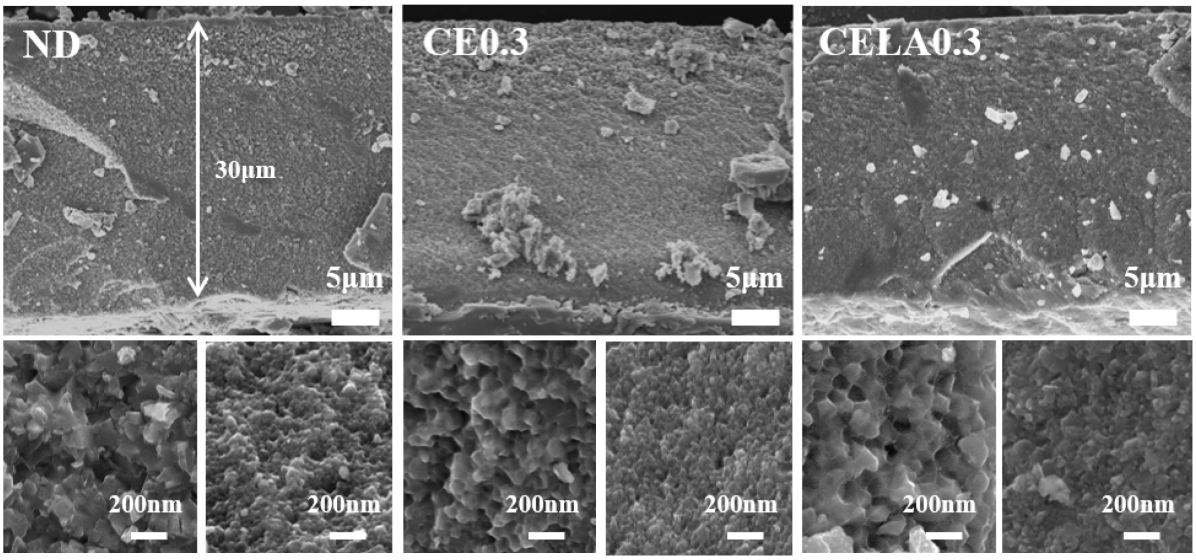

Fig. 2. SEM images of initial melt-spun powders of ND, CE0.3, CELA0.3.

and premagnetized with a 5T pulsing magnetic field parallel to c-axis. The degree of crystallographic alignment of the $Nd_2Fe_{14}B$ magnetic phase was calculated from the remanence measured along the direction parallel and perpendicular to c-axis, respectively.

3. Results and Discussion

Figure 2 shows typical microstructures of initial ND, CE0.3 and CELA0.3 melt-spun powders. The initial melt-spun powders had plate-like shapes, and the typical thickness was about 30 μm. The powders were composed of two distinct areas, that is, ultrafine-grained (approximately 50 nm-sized grains) area and coarse-grained (approximately 100 nm-sized grains), respectively. Especially, the 100 nm-sized grains appeared only in one side of the powder. It could be attributed to the fact that cooling rate was different between two surface sides of powder during single-roller melt-spinning process. In other words, cooling rate of free-side surface was lower than that of wheel-side surface, which resulted in coarse-grained area in the free-side surface. It was reported that the grain size in the fracture surface of melt-spun powders decreased gradually from the free-side surface to wheel-side surface [25]. It should also be noted that this typical microstructure was confirmed regardless of the composition in the initial melt-spun powder. This indicates that the effect of the substitution of Ce and La for Nd on the microstructure of the initial melt-spun powders is negligible.

Figure 3 shows typical XRD patterns of initial ND, CE0.3 and CELA0.3 melt-spun powders. The strongest reflections correspond to the tetragonal 2:14:1 phase

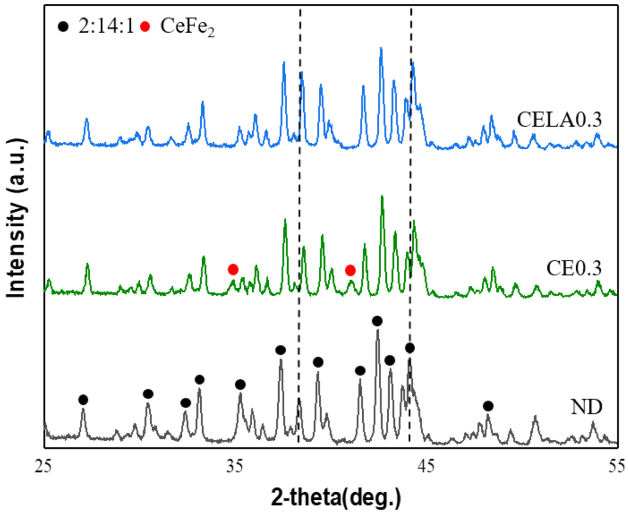

Fig. 3. (Color online) XRD patters of initial powders with different composition.

(space group $P4_2/mnm$) in ND powder. The peaks corresponding to the $CeFe_2$ phase newly appeared in the CE0.3 powder. The appearance of the $CeFe_2$ phase makes a quite difference between the Nd-Fe-B and Ce-Fe-B ternary phase diagram [17]. 1:2 phase could not be formed in Nd-Fe-B system, but inevitably formed in Ce-Fe-B system as shown in Fig. 4. These results have been well reported in sintered magnets [26]. The newly appeared $CeFe_2$ phase in CE0.3 powder disappeared again in CELA0.3 powder as shown in Fig. 3. This indicated that simultaneous substitution of Ce and La for Nd was quite effective for preventing the formation of $CeFe_2$ phase in Nd-lean RE-Fe-B magnets, which is well consistent with previous

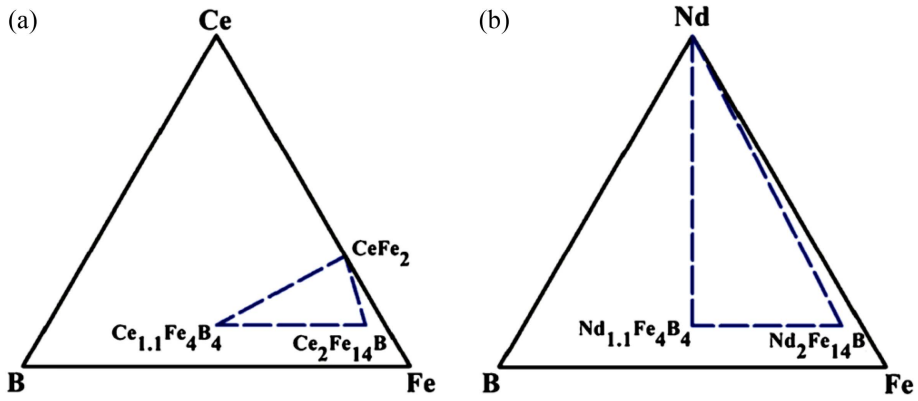

Fig. 4. (Color online) Ternary phase diagram of (a) Ce-Fe-B and (b) Nd-Fe-B system, respectively.

report [27]. On the other hand, the characteristic peaks of 2:14:1 phase in the CE0.3 powder shift toward higher angle compared to those in the ND and CELA0.3 powder. This peak shift of 2:14:1 phase can be explained from difference in atomic radius of rare earth elements. The atomic radius of Nd^{3+} is 98.3 pm, whereas the atomic radius of Ce^{3+} and Ce^{4+} is 102 and 87 pm, respectively [28]. And the Ce in the $Ce_2Fe_{14}B$ phase exhibited the mixed valence of 3.44 due to the coexistence of 3^+ and 4^+, which leaded to the smaller lattice parameters of $Ce_2Fe_{14}B$ (a = 8.76 Å and c = 12.11 Å) than those of $Nd_2Fe_{14}B$ (a = 8.80 Å and c = 12.20 Å) [8]. So the substitution of Ce for Nd in $Nd_2Fe_{14}B$ phase would result in lattice shrinkage, and the obtained XRD peaks would shift to higher angle with increasing Ce content. In addition, the substitution of La in $RE_2Fe_{14}B$ phase would result in the lattice expansion of 2:14:1 phase due to the larger atomic radius (La^{3+} = 103 pm) than Nd and Ce. Especially, the Ce valence are dependent on the steric environment and can lead to the desired Ce^{3+} with expanding site volume. When La is co-doped with the Ce into the $Nd_2Fe_{14}B$ lattice, it can produce lattice expansion and induce the desired Ce^{3+}. Therefore, La/Ce co-doping would induce the valance transition from Ce^{4+} to Ce^{3+}, shifting the peak of 2:14:1 phase toward lower angle [7, 29].

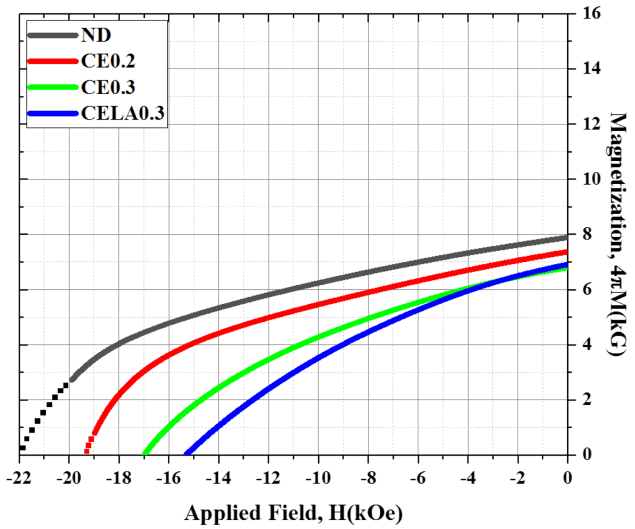

Fig. 5. (Color online) The demagnetization curves of initial melt-spun powders of ND, CE0.2, CE0.3, CELA0.3.

Figure 5 shows the demagnetization curves of initial melt-spun powders with different composition. ND powder showed almost the same remanence and coercivity as the commercial MQU-F powder, 7.8 kG and 22 kOe, respectively. However, the remanence and coercivity gradually decreased with increasing Ce content. Especially, CELA0.3 powder showed lower coercivity but higher remanence than CE0.3 powder. This dependence of magnetic properties on Ce and La content could be ascribed to the magnetic dilution effect that Ce, La substitution for Nd in the 2:14:1 phase decreased the intrinsic magnetic properties. Table 1 shows intrinsic magnetic properties of three 2:14:1 phases. The saturation magnetization of $La_2Fe_{14}B$ was higher than that of $Ce_2Fe_{14}B$, which was the reason why the remanence of CELA0.3 is higher than that of CE0.3 powder.

Figure 6 shows demagnetization curves of hot-deformed magnets produced from four different initial powders. After hot-deformation, the remanence largely increased due to the deformation-induced texture in nanocrystalline 2:14:1 main phase, while the coercivity decreased compared with the corresponding initial powder. It is well

Table 1. The intrinsic magnetic properties of $Nd_2Fe_{14}B$, $Ce_2Fa_{14}B$ and $La_2Fe_{14}B$ phase.

Phase	M_s (kG)	H_a (kOe)	T_c (K)
$Nd_2Fe_{14}B$	16	73	585
$Ce_2Fe_{14}B$	11.7	26	424
$La_2Fe_{14}B$	13.8	20	516

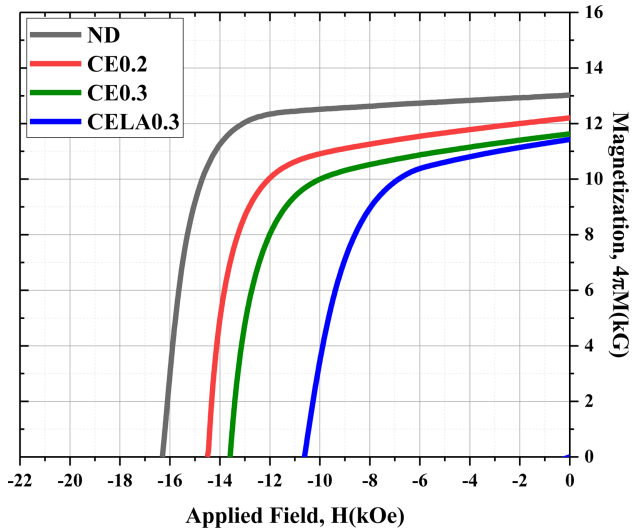

Fig. 6. (Color online) The demagnetization curves of hot-deformed magnets of ND, CE0.2, CE0.3, CELA0.3.

known that hot-deformation causes the alignment of c-axis of grains parallel to the pressing direction. The mechanism of texture formation during hot-deformation process was reported that grains grew along the [010] and [100] axis into platelet shape and the [001] axis of platelet grains were oriented parallel to the pressing direction by the interface-controlled solution-precipitation-creep process and grain boundary sliding [24, 30, 31]. On the other hand, the remanence and coercivity gradually decreased with increasing Ce content due to inferior intrinsic properties of the $Ce_2Fe_{14}B$, which was almost the same tendency as the initial melt-spun powders. The interesting point was that the remanence of hot-deformed CELA0.3 magnet was lower than hot-deformed CE0.3 magnet although the saturation magnetization of $La_2Fe_{14}B$ was

Table 2. The density and degree of alignment of ND, CE0.2, CE0.3 and CELA0.3 estimated from demagnetization curves.

	ND	CE0.2	CE0.3	CELA0.3
Theoretical Density (g/cm^3)	7.59	7.598	7.602	7.58
Density (g/cm^3)	7.576	7.497	7.445	7.304
Relative density (%)	99.8	99	98	96
DoA (%)	83.72	75.64	69.71	61.00

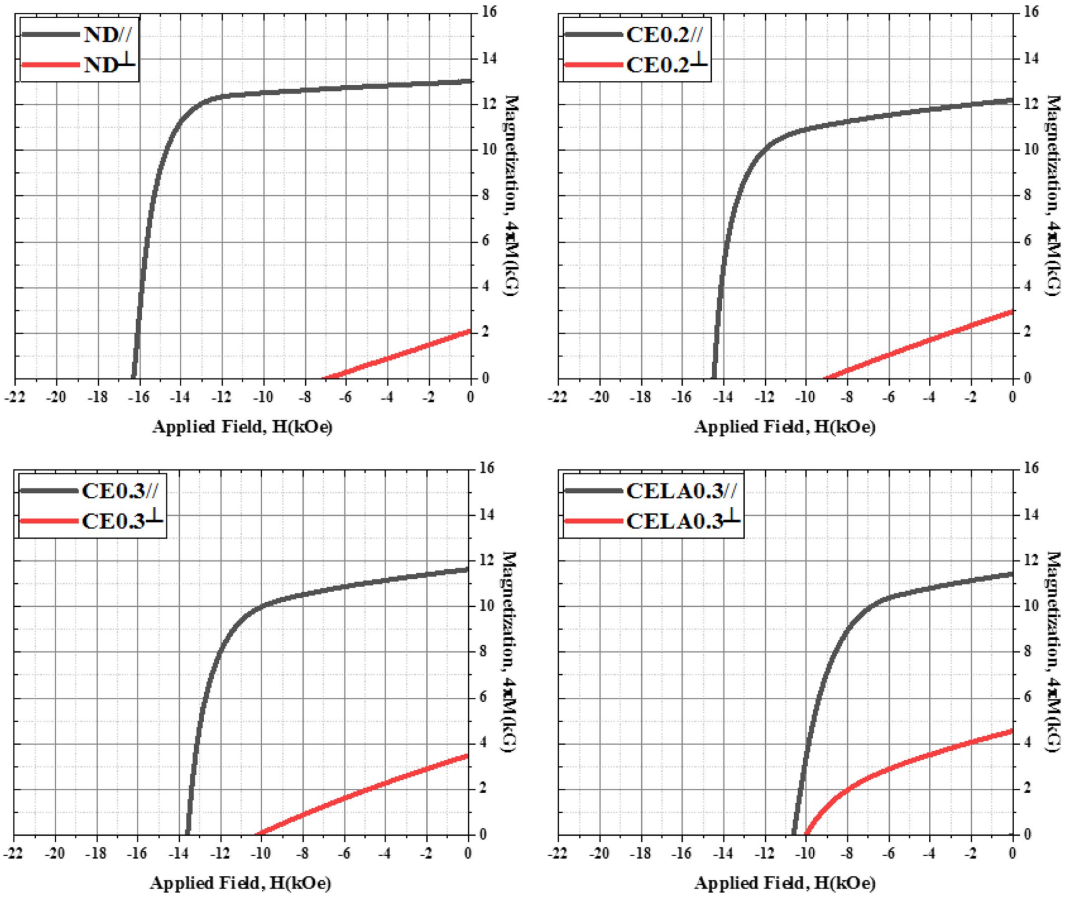

Fig. 7. (Color online) The demagnetization curves of hot-deformed magnets of ND, CE0.2, CE0.3, CELA0.3 with direction parallel and perpendicular to the c-axis.

higher than that of $Ce_2Fe_{14}B$.

In general, the remanence (B_r) can be expressed by equation (1), in which ρ, ρ_0, V_{non}, V_0, M_s, and φ are density, theoretical density, volume of non-magnetic phases, volume of magnet, saturation magnetization and degree of alignment (DoA), respectively [32].

$$B_r = \left(\frac{\rho}{\rho_0}\right)\left(1 - \frac{V_{non}}{V_0}\right) \times M_s \times \varphi \quad (1)$$

This equation indicates that the remanence is influenced by not only saturation magnetization but also density and degree of alignment of magnets. Table 2 shows the density and degree of alignment of four kinds of hot-deformed magnets estimated from demagnetization curves. The density of magnet was decreased with substitute Ce and La content. Especially, the magnet produced form CELA0.3 powder showed the lowest density. The relative density of hot-deformed magnets decreased from 99.8 % to 96 % with Ce and La substitution. The degree of alignment in Table 2 was estimated from the following equation (2), where $B_{r\parallel}$ and $B_{r\perp}$ was the remanence measured in the direction parallel (easy) and perpendicular (hard) to pressing direction, respectively [33].

$$DoA = (B_{r\parallel} - B_{r\perp})/B_{r\parallel} \times 100 \quad (2)$$

Figure 7 shows the demagnetization curves of hot-deformed magnets measured in the direction parallel (easy) and perpendicular (hard) to pressing direction. The degree of alignment was decreased with increasing Ce and La content. Especially, the degree of alignment of CELA0.3 was much lower than that of CE0.3. To obtain high density and degree of alignment of hot-deformed magnet, wettability and melting point of RE-rich phase plays an important role [34, 35]. However, the Ce addition can deteriorate the wettability of RE-rich phase [36]. Furthermore, the melting point of $CeFe_2$ phase, which inevitably forms at grain boundary and triple junction of the Nd-Ce-Fe-B magnet with high Ce content, is 1198 K [10]. It is much higher than hot-deformation temperature, 973 K. Therefore, it seems that the decrease in density and degree of alignment with addition of Ce in RE-Fe-B magnet is due to the low wettability of RE-rich phase and existence of $CeFe_2$ at grain boundaries. Regarding with addition of La, Jin *et al.* reported that the addition of La also deteriorated the wettability of RE-rich phase, forming the hcp-RE_2O_3 phase which mainly distributed as precipitate at the triple junctions in Nd-La-Fe-B magnets [37, 38]. In addition, Tang *et al.* reported that the formation of holes and cracks could be formed in the sintered Nd-Fe-B magnet after adding La due to the low wettability of RE-rich phase, decreasing the density and magnetic properties [5, 39]. Based upon these results, it seems that the remanence of hot-deformed Nd-Fe-B magnet decreased due to the effect of not only decline in saturation magnetization due to intrinsic magnetic properties but also deterioration in the density and the degree of alignment by substitution of Ce and La for Nd in Nd-Fe-B magnet. For the high density and degree of alignment, secondary phase and wettability of grain boundary phase must be improved before or during hot-deformation.

Figure 8 shows maximum energy product ($(BH)_{max}$) and cost performance (defined as $(BH)_{max}$/cost) of the hot-deformed magnets, respectively. The $(BH)_{max}$ gradually decreased with increasing Ce and La content. Especially, CELA0.3 showed the lowest value. However, the cost performance was largely enhanced from 2.32 to 2.62 MGOe×kg/$ by 13 % when increasing the content of Ce substituted for Nd from 0 to 0.3 wt.%. Although the cost performance was lower compared to that of CE0.3 magnet,

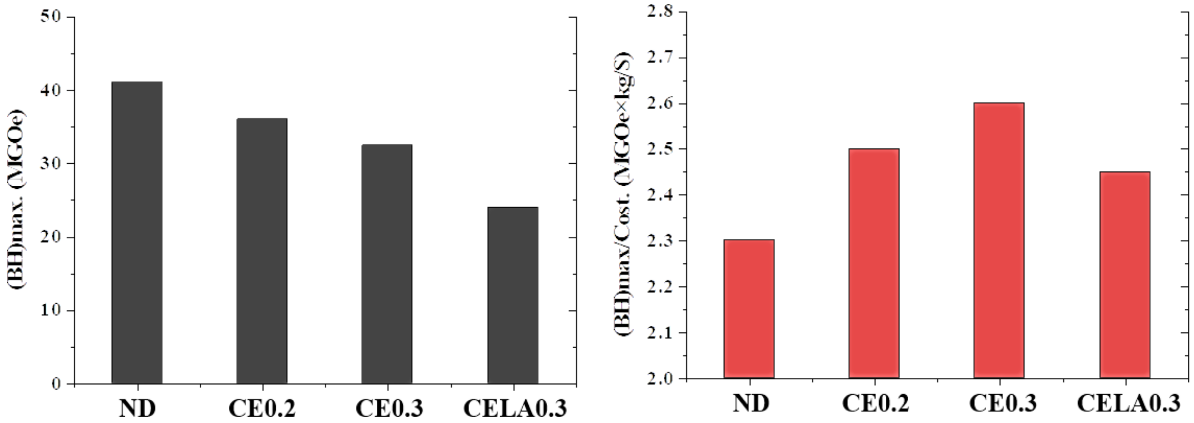

Fig. 8. (Color online) Maximum energy product ($(BH)_{max}$) and cost performance (defined as $(BH)_{max}$/cost) of the hot-deformed magnets of ND, CE0.2, CE0.3, CELA0.3.

the CELA0.3 magnet also showed higher cost performance than that of ND magnet. It suggests that low-cost M(Ce, La) element can be used to fabricate high cost-performance Nd-lean RE-Fe-B hot-deformed magnets.

4. Conclusion

The effects of the Ce and La substitution for Nd on magnetic properties of Nd-Fe-B hot-deformed magnets have been investigated. The results show that the microstructure of the initial melt-spun powders was independent on the composition. In the case of the initial melt-spun powders, $CeFe_2$ phase appeared in the CE0.3 and disappeared again in CELA 0.3. After hot-deformation, the magnetic properties were decreased with increasing Ce and La content due to the inferior intrinsic magnetic properties of 2:14:1 phase, which was almost the same tendency as initial melt-spun powder. In particular, CELA0.3 showed lower remanence than CE0.3 after hot-deformation although the intrinsic magnetization of $La_2Fe_{14}B$ phase is higher than that of $Ce_2Fe_{14}B$ phase. It is because that the relative density and degree of alignment of CELA0.3 was lowest among four samples employed in this study. On the other hand, although the $(BH)_{max}$ decreased by substitution of Ce and La, the cost performance was enhanced from 2.32 to 2.62 MGOe×kg/$ by 13 % when increasing the content of Ce substituted for Nd from 0 to 0.3 wt.%.

Acknowledgements

This work was supported by Ministry of Trade, Industry and Energy, South Korea, through the Industrial Strategic Technology Development Program under Grant 20000401, 10080382.

References

[1] O. Gutfleisch, M. A. Willard, E. Brück, C. H. Chen, S. G. Sankar, and J. P. Liu, Advanced Materials **23**, 821 (2011).
[2] S. Sugimoto, J. Phys. D: Appl. Phys. **44**, 064001 (2011).
[3] J. G. Lee, J. H. Yu, H. J. Kim, and T. S. Jang, J. Korean Magn. Soc. **22**, 58 (2012).
[4] Wei Li, Anhua Li, Haibo Feng, Shulin Huang, Jingdai Wang, and Minggang Zhu, IEEE Trans. Magn. **51**, 1 (2015).
[5] X. Fan, G. Ding, R. Chen, K. Chen, S. Guo, C. You, D. Lee, and A. Yan, Acta Materialia **154**, 343 (2018).
[6] K. Chen, S. Guo, X. D. Fan, G. F. Ding, J. H. Di, R. J. Chen, and A. R. Yan, J. Magn. Magn. Mater. **457**, 135 (2018).
[7] J. Jin, Y. Zhang, G. Bai, Z. Qian, C. Wu, T. Ma, B. Shen, and M. Yan, Scientific Reports **6**, 30194 (2016).
[8] J. F Herbst, Rev. Mod. Phys. **63**, 4 (1991).
[9] J. Jin, T. Ma, Y. Zhang, G. Bai, and M. Yan, Scientific Reports **6**, 32200 (2016).
[10] Y. Zhang, T. Ma, J. Jin, J. Li, C. Wu, B. Shen, and M. Yan, Acta Materialia **128**, 22 (2017).
[11] J. Jin, M. Yan, T. Ma, W. Li, Y. Liu, Z. Zhang, and S. Fu, Materials & Design **186**, 108308 (2020).
[12] E. Niu, Z. Chen, G. Chen, Y. Zhao, J. Zhang, X. Rao, B. Hu, and Z. Wang, J. Appl. Phys. **115**, 113912 (2014).
[13] J. F. Herbst, M. S. Meyer, and F. E. Pinkerton, J. Appl. Phys. **111**, 7 (2012).
[14] C. H. Chiu and H. W. Chang, J. Appl. Phys. **99**, 518 (2006).
[15] A. K. Pathak, M. Khan, K. A. Gschneidner Jr, R. W. McCallum, L. Zhou, K. Sun, K. W. Dennis, C. Zhou, F. E. Pinkerton, M. J. Kramer, and V. K. Pecharsky, Advanced Materials **27**, 2663 (2015).
[16] C. Yan, S. Guo, R. Chen, D. Lee, and A. Yan, IEEE Trans. Magn. **50**, 1 (2014).
[17] Q. Jiang and Z. Zhong, Journal of Materials Science & Technology **33**, 1087 (2017).
[18] K. Hono and H. Sepehri-Amin, Scripta Materialia **67**, 530 (2012).
[19] W. Li, S. Hirosawa, K. Hono, T. Ohkubo, and T. Nishiuchi, J. Appl. Phys. **105**, 07A706 (2009).
[20] H. Sepehri-Amin, T. Ohkubo, T. Nishiuchi, S. Hirosawa, and K. Hono, Scripta Materialia **63**, 1124 (2010).
[21] D. N. Brown, Z. Wu, F. He, D. J. Miller, and J. W. Herchenroeder, J. Phys. **26**, 064202 (2014).
[22] C. Jin, R. Chen, X. Tang, J. Ju, W. Yin, Z. Wang, M. Li, D. Lee, and A. Yan, J. Magn. Magn. Mater. **449**, 313 (2018).
[23] X. Tang, H. Sepehri-Amin, M. Matsumoto, T. Ohkubo, and K. Hono, Acta Materialia **175**, 1 (2019).
[24] H. R. Cha, S. Liu, J. H. Yu, H. W. Kwon, Y. D. Kim, and J. G. Lee, IEEE Trans. Magn. **51**, 1 (2015).
[25] L. Bin, L. Yanfeng, W. Huijie, L. Anhua, Z. Minggang, L. Wei, and Z. Yue, Jounal of Rare Earths **32**, 514 (2014).
[26] E. Niu, Z. Chen, G. Chen, Y. Zhao, J. Zhang, X. Rao, B. Hu, and Z. Wang, J. Appl. Phys. **115**, 113912 (2014).
[27] W. Liu, Z. Zhang, M. Yue, Z. Li, D. Zhang, and H. Zhang, J. Magn. Magn. Mater. **64**, 61 (2018).
[28] M. Yang, L. Yang, B. Yang, H. Wang, Y. Hu, and A. Maclennan, J. Alloys Compd. **710**, 519 (2017).
[29] A. Alam and D. D. Johnson, Physical Review B **89**, 235126 (2014).
[30] H. Y. Yasuda, M. Kumano, T. Nagase, R. Kato, and H. Shimizu, Scripta Materialia **65**, 743 (2011).
[31] W. Grünberger, D. Hinz, A. Kirchner, K. Müller, and L. Schultz, J. Alloys Compd. **257**, 293 (1997).
[32] D. N. Brown, Y. K. Lim, R. A. Remoroza, and D. J. Miller, J. Appl. Phys. **109**, 07A742 (2011).
[33] H. Cha, J. Yu, Y. Baek, H. Kwon, T. Kim, C. Yang, T.

Lim, Y. Kim, and J. Lee, Met. Mater. Int. **20**, 909 (2014).
[34] S. Huang, H. Feng, M. Zhu, A. Li, Y. Li, Y. Sun, Y. Zhang, and W. Li, International Journal of Minerals, Metallurgy, and Materials **22**, 417 (2015).
[35] Z. Jing, Z. Guo, Y. He, M. Li, W. Li, M. Zhang, and M. Zhu, J. Magn. Magn. Mater. **488**, 165353 (2019).
[36] C. Kan, G. Shuai, F. Xiaodong, D. Guangfei, C. Ling, C. Renjie, L. Don, and Y. Aru, Jounal od Rare Earths **35**, 158 (2017).
[37] J. Jin, Z. Wang, G. Bai, B. Peng, Y. Liu, and M. Yan, J. Alloys Compd. **749**, 580 (2018).
[38] W. Mo, L. Zhang, Q. Liu, A. Shan, J. Wu, and M. Komuro, Scripta Materialia **59**, 179 (2008).
[39] W. Tang, Y. Q. Wu, K. W. Dennis, N. T. Oster, M. J. Kramer, I. E. Anderson, and R. W. McCallum, J. Appl. Phys. **109**, 07A704 (2011).